Selected for a Viewpoint in *Physics*

PHYSICAL REVIEW A **79**, 033621 (2009)

Dissipation-induced coherence and stochastic resonance of an open two-mode Bose-Einstein condensate

D. Witthaut,[1,*] F. Trimborn,[2] and S. Wimberger[3]

[1]*QUANTOP, Niels Bohr Institute, University of Copenhagen, DK-2100 Copenhagen, Denmark*

[2]*Institut für Mathematische Physik, TU Braunschweig, D-38106 Braunschweig, Germany*

[3]*Institut für Theoretische Physik, Universität Heidelberg, D-69120 Heidelberg, Germany*

(Received 27 October 2008; published 23 March 2009)

We discuss the dynamics of a Bose-Einstein condensate in a double-well trap subject to phase noise and particle loss. The phase coherence of a weakly interacting condensate, experimentally measured via the contrast in an interference experiment, as well as the response to an external driving becomes maximal for a finite value of the dissipation rate matching the intrinsic time scales of the system. This can be understood as a stochastic resonance of the many-particle system. Even stronger effects are observed when dissipation acts in concurrence with strong interparticle interactions, restoring the purity of the condensate almost completely and increasing the phase coherence significantly. Our theoretical results are backed by Monte Carlo simulations, which show a good qualitative agreement and provide a microscopic explanation for the observed stochastic resonance effect.

DOI: 10.1103/PhysRevA.79.033621 PACS number(s): 03.75.Lm, 03.75.Gg, 03.65.Yz

I. INTRODUCTION

Stochastic resonance (SR) is a strongly surprising yet very general effect in nonlinear dynamical systems. Against our naive understanding, the response of a system to an external driving can be facilitated if an appropriate amount of noise is added. In fact, the maximum of the response—the stochastic resonance—is found if the time scale of the noise matches an intrinsic time scale of the system. The effect was first described for strongly damped classical systems such as the overdamped particle in a driven double-well trap. In this case the noise is strong enough to induce the transition between the wells, whereas it is still weak enough not to randomize the dynamics completely. The particle will then hop to and fro almost deterministically if the average transition time between the wells due to the noise equals half of the driving period [1]. By now, a stochastic resonance has been shown in a variety of systems; an overview can be found in the review articles [2–5]. In addition to numerous examples in classical dynamics, stochastic resonance has also been found in a variety of quantum systems (see, e.g., [5–11]).

Recently, there has been an increased interest in the effects of dissipation and the possibilities to control these in interacting many-body quantum systems. For instance, the entanglement in a spin chain assumes an SR-like maximum for a finite amount of thermal noise [12]. Methods to attenuate phase noise for an open two-mode Bose-Einstein condensate (BEC) were discussed in [13], and the effects of particle loss on the spin squeezing of such a system were analyzed in [14]. Furthermore, it has been shown that dissipative processes can be tailored to prepare arbitrary pure states for quantum computation and strongly correlated states of ultracold atoms [15,16] or to implement a universal set of quantum gates [17]. Actually, a recent experiment has even proven that strong inelastic collisions may inhibit particle losses and induce strong correlations in a quasi-one-dimensional (quasi-1D) gas of ultracold atoms [18,19].

In the present paper, we investigate the effects of noise and dissipation for a BEC in a double-well trap. The essential idea has been introduced in a recent letter [20], and here we extend the discussion to a detailed analysis of the predicted SR phenomenon. The setup under consideration has been experimentally realized by several groups only in the last few years [21–26]. Ultracold atoms in optical potentials have the enormous advantage that they allow us to observe the quantum dynamics of an interacting many-particle system *in situ*. Thus they serve as excellent model systems, bringing together aspects of nonlinear dynamics, solid-state physics, and the theory of open quantum systems. Here we show that the coherence of the two condensate modes assumes a maximum in the fashion of the stochastic resonance effect for a finite dissipation rate, which matches the time scales of the intrinsic dynamics. In this case the particle loss is strong enough to significantly increase the condensate purity, whereas it is still weak enough not to dominate the dynamics completely. Similarly the response to an external driving is increased if a proper amount of dissipation is present. Even more remarkable results are found when dissipation acts in concurrence with strong interparticle interactions, leading to an almost complete revival of the purity of the BEC. These effects are of considerable strength for realistic parameters and thus should be readily observable in ongoing experiments.

This paper is organized as follows. First, we introduce the theoretical description of the open two-mode Bose-Hubbard system. We discuss the main sources of noise and dissipation and derive the corresponding mean-field approximation of the many-particle system. The resulting dynamics for weak interparticle interactions is analyzed in Sec. III. It is shown that the phase contrast between the two modes assumes an SR-like maximum if the time scales of tunneling and dissipation are matched. This result is explained within the mean-field approximation as well as for the underlying many-

*dirk.witthaut@nbi.dk

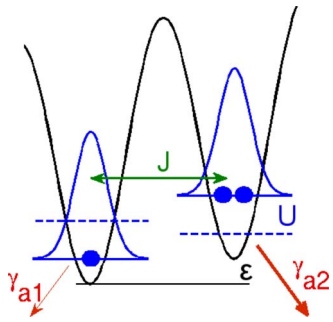

FIG. 1. (Color online) The open double-well trap considered in the present paper.

particle quantum dynamics with Monte Carlo simulations backing up the approximative results. The response of the open system to an external driving is discussed in Sec. IV. The amplitude of the forced oscillation also shows a pronounced stochastic resonance effect. Section V then investigates the case of a strongly interacting BEC, which is a problem of both fundamental theoretical interest as well as high experimental relevance. The interplay between interactions and dissipation can restore the purity of the condensate almost completely and significantly increase the phase coherence in comparison with situations where one of the two is weak or missing. This counterintuitive effect is robust and can be explained by the appearance of novel nonlinear eigenstates.

II. NOISE AND DISSIPATION IN A TRAPPED BEC

The basic setup under consideration is depicted in Fig. 1. Ultracold atoms are confined in a double-well trap that can be realized, e.g., by superimposing an optical lattice with an optical dipole trap [21–23], in a bichromatic optical lattice [24,25], or on an atom chip [26]. We consider the case of a deep but tight trap, which is tuned such that only one mode in each well is bounded and thus significantly populated. All scattering solutions of the model form a continuum of unbound modes which adds up to the heat bath (see below) [27]. One major assumption in the derivation of this model is that the level spacing between the trap modes is significantly larger than the self-energy of the atom-atom interactions in the trap: $UN \ll \hbar\omega_{\text{trap}}$. For a typical trap frequency around 100 Hz, this restricts the atom number to a few hundreds. Note that this model is not compatible to the Thomas-Fermi approximation, where the many-body interaction dominates the kinetic energy. Likewise, it is not directly applicable to the case of two weakly coupled 1D quasicondensates [28,29] due to the excitation of longitudinal modes.

The unitary dynamics of the atoms is then described by the two-mode Bose-Hubbard Hamiltonian [30–33],

$$\hat{H} = -J(\hat{a}_1^\dagger \hat{a}_2 + \hat{a}_2^\dagger \hat{a}_1) + \epsilon_2 \hat{n}_2 + \epsilon_1 \hat{n}_1 + \frac{U}{2}[\hat{n}_1(\hat{n}_1 - 1) + \hat{n}_2(\hat{n}_2 - 1)], \tag{1}$$

which describes both the dynamics of the condensed fraction, as well as the noncondensate, but nevertheless trapped atoms. The operators $\hat{a}_j$ and $\hat{a}_j^\dagger$ are the bosonic annihilation and creation operators in mode j and $\hat{n}_j = \hat{a}_j^\dagger \hat{a}_j$ is the corresponding number operator. Furthermore, J denotes the tunneling matrix element between the wells, U denotes the interaction strength, and ϵ_j denotes the on-site energy of the jth well. We set $\hbar = 1$, thus measuring all energies in frequency units.

In order to clarify the algebraic structure of the model and to analyze the dynamics in the Bloch representation we introduce the collective operators,

$$\hat{L}_x = \frac{1}{2}(\hat{a}_1^\dagger \hat{a}_2 + \hat{a}_2^\dagger \hat{a}_1),$$

$$\hat{L}_y = \frac{i}{2}(\hat{a}_1^\dagger \hat{a}_2 - \hat{a}_2^\dagger \hat{a}_1),$$

$$\hat{L}_z = \frac{1}{2}(\hat{a}_2^\dagger \hat{a}_2 - \hat{a}_1^\dagger \hat{a}_1), \tag{2}$$

which form an angular-momentum algebra su(2) with quantum number $\ell = N/2$ [30–35], where N is the actual particle number. Hamiltonian (1) then can be rewritten as

$$\hat{H} = -2J\hat{L}_x + 2\epsilon \hat{L}_z + U\hat{L}_z^2 \tag{3}$$

up to terms only depending on the total number of atoms. Here, $\epsilon = \epsilon_2 - \epsilon_1$ denotes the difference of the on-site energies of the two wells.

A model for noise and dissipation in a deep trapping potential has been derived by Anglin [27] and later extended by Ruostekoski and Walls [36] to the case of two weakly coupled modes. The dissipation of energy is described by the coupling to a thermal reservoir consisting of noncondensate modes. The dynamics is then given by the master equation,

$$\dot{\hat{\rho}} = -i[\hat{H}, \hat{\rho}] - \frac{\gamma_p}{2} \sum_{j=1,2} (\hat{n}_j^2 \hat{\rho} + \hat{\rho} \hat{n}_j^2 - 2\hat{n}_j \hat{\rho} \hat{n}_j) - \frac{\gamma_{\text{in}}}{2} \sum_{j=1,2;\pm} (\hat{C}_{j\pm}^\dagger \hat{C}_{j\pm} \hat{\rho} + \hat{\rho} \hat{C}_{j\pm}^\dagger \hat{C}_{j\pm} - 2\hat{C}_{j\pm} \hat{\rho} \hat{C}_{j\pm}^\dagger) \tag{4}$$

with the Lindblad operators

$$\hat{C}_{j+} = \hat{a}_j^\dagger$$

and

$$\hat{C}_{j-} = e^{\beta/2(\epsilon_j - \mu + U\hat{n}_j)} \hat{a}_j, \tag{5}$$

describing growth and depletion of the condensate.

Let us briefly discuss the effects of the noise and dissipation terms. The second term $\sim \gamma_p$ in Eq. (4) describes phase noise due to elastic collisions with the background gas atoms. It is usually the dominating contribution, effectively heating the system, but leaving the total particle number invariant. If only phase noise is present, the system relaxes to an equilibrium state where all coherences are lost and all Dicke states $|n_1, N-n_1\rangle \sim \hat{a}_1^{\dagger n_1} \hat{a}_2^{\dagger N-n_1} |0,0\rangle$ are equally populated,

$$\langle n_1, N-n_1|\hat{\rho}|n_1', N-n_1'\rangle = \frac{1}{N+1}\delta_{n_1,n_1'}, \tag{6}$$

as long as $J \neq 0$ [37,38]. This corresponds to a thermal state of infinite temperature with $\langle \hat{\mathbf{L}} \rangle = \mathbf{0}$. The remaining terms $\sim \gamma_{\text{in}}$ in the master equation [Eq. (4)] describe amplitude noise, i.e., the growth and depletion of the condensate due to inelastic collisions with the background gas. In contrast to phase noise, amplitude noise heats *and* cools the system. If both amplitude and phase noise are present, the system will relax to the proper thermal state with a density operator $\hat{\rho} \propto \exp[-\beta(\hat{H} - \mu\hat{n})]$ [27].

In current experiments amplitude noise and dissipation are usually extremely weak in comparison to phase noise [36], if it is not introduced artificially as for example by forced evaporative cooling during the preparation of the BEC. For example, phase noise damps Josephson oscillations on a time scale of a few hundred milliseconds in the experiments, while less than 10% of the atoms are lost during a 30 s experiment [21–23]. This is much too weak to produce significant effects, such that the terms describing the particle exchange with the background gas in Eq. (4) can be neglected, $\gamma_{\text{in}} \approx 0$.

However, nontrivial effects of dissipation such as the stochastic resonance discussed below require strong, tunable, and biased loss rates. A well-controllable source of dissipation can be implemented artificially by shining a resonant laser beam onto the trap, which removes atoms with the site-dependent rates γ_{aj} from the two wells $j=1,2$. For such a laser beam focused on one of the wells an asymmetry of $f_a = (\gamma_{a2} - \gamma_{a1})/(\gamma_{a2} + \gamma_{a1}) = 0.5$ should be feasible. In magnetic trapping potentials, a similar effect can also be achieved by a forced rf transition to an untrapped magnetic substate [39].

Therefore the above master equation must be extended to take into account the single-particle losses. The additional term describing the particle loss is well established and routinely used in the context of photon fields [38]. In the following we will thus consider the dynamics generated by the master equation:

$$\dot{\hat{\rho}} = -i[\hat{H}, \hat{\rho}] - \frac{\gamma_p}{2}\sum_{j=1,2}(\hat{n}_j^2\hat{\rho} + \hat{\rho}\hat{n}_j^2 - 2\hat{n}_j\hat{\rho}\hat{n}_j)$$
$$- \frac{1}{2}\sum_{j=1,2}\gamma_{aj}(\hat{a}_j^\dagger\hat{a}_j\hat{\rho} + \hat{\rho}\hat{a}_j^\dagger\hat{a}_j - 2\hat{a}_j\hat{\rho}\hat{a}_j^\dagger). \tag{7}$$

The macroscopic dynamics of the atomic cloud is to a very good approximation [32,33,40] described by a mean-field approximation, considering only the expectation values $s_j(t) = 2\,\text{tr}[\hat{L}_j\hat{\rho}(t)]$ of the angular-momentum operators [Eq. (2)] and the particle number $n(t) = \text{tr}[(\hat{n}_1 + \hat{n}_2)\hat{\rho}(t)]$. The evolution equations for the Bloch vector $\mathbf{s} = (s_x, s_y, s_z)$ are then calculated starting from the master equation via $\dot{s}_j = 2\,\text{tr}(\hat{L}_j\dot{\hat{\rho}})$ with the exact result (cf. [40]),

$$\dot{s}_x = -2\epsilon s_y - U(s_y s_z + \Delta_{yz}) - T_2^{-1}s_x,$$

$$\dot{s}_y = 2Js_z + 2\epsilon s_x + U(s_x s_z + \Delta_{xz}) - T_2^{-1}s_y,$$

$$\dot{s}_z = -2Js_y - T_1^{-1}s_z - T_1^{-1}f_a n,$$

$$\dot{n} = -T_1^{-1}n - T_1^{-1}f_a s_z, \tag{8}$$

where we have defined the transversal and longitudinal damping times by

$$T_1^{-1} = (\gamma_{a1} + \gamma_{a2})/2 \quad \text{and} \quad T_2^{-1} = \gamma_p + T_1^{-1}. \tag{9}$$

These equations of motion resemble the celebrated Bloch equations in nuclear-magnetic resonance [41,42], with some subtle but nevertheless important differences. The longitudinal relaxation is now associated with particle loss and, more important, the dynamics is substantially altered by the U-dependent interaction term [21,30,31].

The exact equations of motion (8) still include the covariances

$$\Delta_{jk} = \langle \hat{L}_j\hat{L}_k + \hat{L}_k\hat{L}_j\rangle - 2\langle \hat{L}_j\rangle\langle \hat{L}_k\rangle. \tag{10}$$

The celebrated mean-field description is now obtained by approximating the second-order moments by products of expectation values such that $\Delta_{jk} \approx 0$ [30–33].

In the following, we will show that a finite amount of dissipation induces a maximum of the coherence which can be understood as a stochastic resonance effect. In this discussion we have to distinguish between two different kinds of coherence, which will both be considered in the following. First of all we consider the phase coherence between the two wells, which is measured by the average *contrast* in interference experiments as described in [21–23] and given by

$$\alpha(t) = \frac{2|\langle \hat{a}_1^\dagger\hat{a}_2\rangle|}{\langle \hat{n}_1 + \hat{n}_2\rangle} = \frac{\sqrt{s_x(t)^2 + s_y(t)^2}}{n(t)}. \tag{11}$$

Second, we will analyze how close the many-particle quantum state is to a pure Bose-Einstein condensate. This property is quantified by the purity

$$p = 2\,\text{tr}(\hat{\rho}_{\text{red}}^2) - 1 \tag{12}$$

of the reduced single-particle density matrix [32,33,35,43],

$$\hat{\rho}_{\text{red}} = \frac{1}{N}\begin{pmatrix} \langle \hat{a}_1^\dagger\hat{a}_1\rangle & \langle \hat{a}_1^\dagger\hat{a}_2\rangle \\ \langle \hat{a}_2^\dagger\hat{a}_1\rangle & \langle \hat{a}_2^\dagger\hat{a}_2\rangle \end{pmatrix}. \tag{13}$$

One can easily show that the purity is related to the Bloch vector $\mathbf{s}$ by $p = |\mathbf{s}|^2/n^2$. A pure BEC, corresponding to a product state, is, of course, characterized by $p=1$. For smaller values of p, there is a growing amount of trapped but noncondensate atoms. This depletion of the BEC results from the many-particle interactions, which destroy the macroscopic product state. However, in leading order these do not lead to scattering to the background gas or to higher unpopulated modes, respectively (cf. [27,36]).

III. DISSIPATION-INDUCED COHERENCE IN A WEAKLY INTERACTING BEC

In this section, we show that a proper amount of dissipation can indeed increase the phase coherence (11) of a two-mode BEC similar to the stochastic resonance effect. For simplicity, we start with the linear case $U=0$, where the

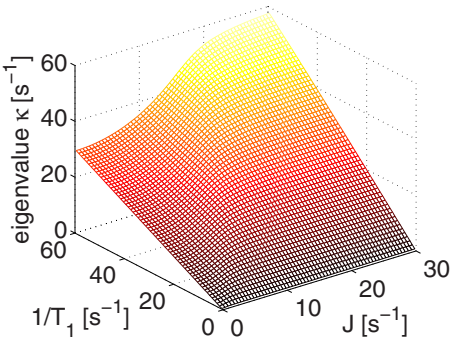

FIG. 2. (Color online) Decay rate κ of the quasi-steady-state (14) as a function of the tunneling rate J and the dissipation rate $1/T_1$ for $\gamma_p=5\ \mathrm{s}^{-1}$ and $U=\epsilon=0$.

mean-field equations of motion for the expectation values [Eq. (8)] are exact. The linear equations resemble the Bloch equations for driven nuclear spins in the rotating wave approximation [42], which are known to show a pronounced stochastic resonance effect [41]: the amplitude of forced oscillations of the spins given by s_y assumes a maximum for a finite value of the relaxation rates T_1^{-1} and T_2^{-1}, provided these are coupled. For the two-mode BEC considered here this is automatically the case as given by Eq. (9). Thus we also expect a maximum of the steady-state value of the phase coherence (11) for a finite value of T_1^{-1}.

Let us now determine the steady-state value of the contrast (11) which quantifies the phase coherence of the two wells as a function of the system parameters and the relaxation rates. Obviously, the only steady state in the strict sense is given by $\mathbf{s}=\mathbf{0}$ and $n=0$, corresponding to a completely empty trap. However, the system rapidly relaxes to a quasi-steady-state where the internal dynamics is completely frozen out and all components of the Bloch vector and the particle number decay at the same rate,

$$\mathbf{s}(t)=\mathbf{s}_0 e^{-\kappa t}, \quad n(t)=n_0 e^{-\kappa t}. \tag{14}$$

Substituting this ansatz into the equations of motion (8), the quasi-steady-state is determined by the eigenvalue equation,

$$\mathbf{M}\begin{pmatrix} s_{x0} \\ s_{y0} \\ s_{z0} \\ n_0 \end{pmatrix} = \kappa \begin{pmatrix} s_{x0} \\ s_{y0} \\ s_{z0} \\ n_0 \end{pmatrix} \tag{15}$$

with the matrix

$$\mathbf{M}=\begin{pmatrix} T_2^{-1} & 2\epsilon & 0 & 0 \\ -2\epsilon & T_2^{-1} & -2J & 0 \\ 0 & 2J & T_1^{-1} & f_a T_1^{-1} \\ 0 & 0 & f_a T_1^{-1} & T_1^{-1} \end{pmatrix}, \tag{16}$$

which is readily solved numerically.

Figure 2 depicts the smallest real eigenvalue κ corresponding to the most stable quasi-steady-state as a function of J and $1/T_1$ for the noninteracting case and $\epsilon=0$. It determines the basic time scale of the system and is essentially proportional to the dissipation rate T^{-1}.

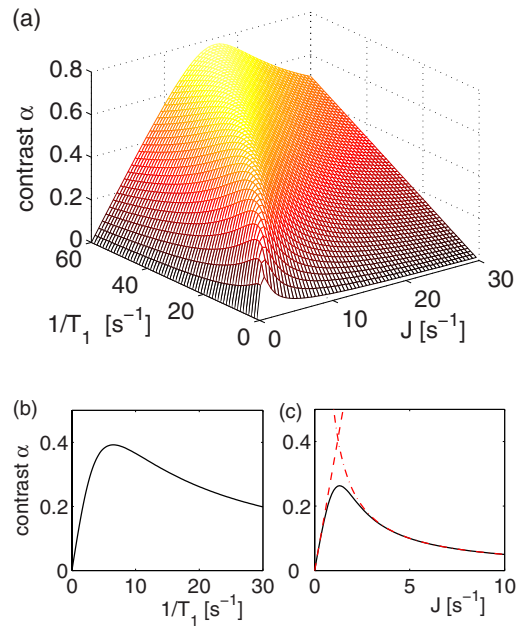

FIG. 3. (Color online) Contrast α of the quasi-steady-state (14) as a function of the tunneling rate J and the dissipation rate $1/T_1$ (a) for $\gamma_p=5\ \mathrm{s}^{-1}$ and $U=\epsilon=0$ and (b) for a fixed value of the tunneling rate $J=2\ \mathrm{s}^{-1}$ and (c) a fixed value of the dissipation rate $1/T_1=2\ \mathrm{s}^{-1}$. The dashed-dotted red lines represent the approximations [Eq. (19)] for small and large values of J.

Figure 3 shows the resulting values of the contrast α as a function of the dissipation rate T_1^{-1} and the tunneling rate J for $U=\epsilon=0$ and $\gamma_p=5\ \mathrm{s}^{-1}$. For a fixed value of one of the parameters, say J, one observes a typical SR-like maximum of the contrast for a finite value of the dissipation rate $1/T_1$ as shown in part (b) of the figure. In particular, the contrast is maximal if the time scales of the tunneling and the dissipation are matched according to

$$4J^2 \approx f_a^2 T_1^{-2} + f_a \gamma_p T_1^{-1}. \tag{17}$$

Furthermore, the contrast $\alpha(J)$ shows a similar maximum for a finite value of the tunneling rate J when the dissipation rate is fixed as shown in Fig. 3(c). Contrary to our intuition this shows that an increase in the coupling of two modes can indeed *reduce* their phase coherence.

In the special case $\epsilon=0$, illustrated in Fig. 3, one can solve the eigenvalue problem [Eq. (15)] exactly. In this case one has $s_x=0$ and the contrast α is related to the eigenvalue κ by

$$\alpha=\frac{2J(T_1^{-1}-\kappa)}{f_a T_1^{-1}(T_2^{-1}-\kappa)}. \tag{18}$$

Evaluating the roots of the characteristic polynomial to determine κ leads to an algebraic equation of third order which can be solved analytically. The resulting expressions are quite lengthy, but the limits for small and large values of the tunneling rate are readily obtained as

$$\alpha \approx \frac{2J}{T_2^{-1}-(1-f_a)T_1^{-1}} \quad \text{for } J \ll T_1^{-1},$$

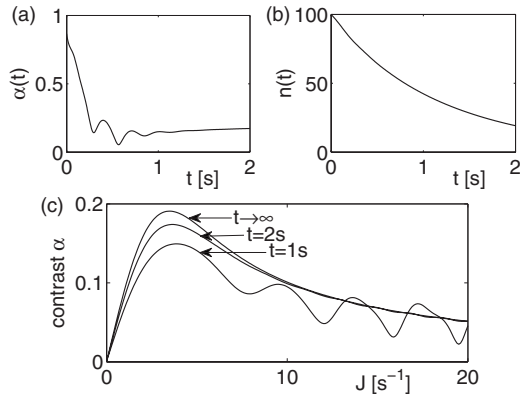

FIG. 4. Relaxation to the quasi-steady-state for $\gamma_p=5\ \mathrm{s}^{-1}$, $T_1^{-1}=1\ \mathrm{s}^{-1}$, $\epsilon=10\ \mathrm{s}^{-1}$, and $U=0$. (a) Relaxation of the contrast $\alpha(t)$ for $J=4\ \mathrm{s}^{-1}$. (b) Decay of the particle number $n(t)$ for $J=4\ \mathrm{s}^{-1}$. (c) Development of the SR maximum of the contrast $\alpha(J)$.

$$\alpha \approx \frac{f_a T_1^{-1}}{2J} \quad \text{for } J \gg T_1^{-1}. \tag{19}$$

These approximations are plotted as dashed red lines in Fig. 3(c). Their intersection given by Eq. (17) gives a very good approximation for the position of the SR-like maximum of the contrast $\alpha(J)$.

An important experimental issue is the question whether the quasi-steady-state is reached fast enough, such that the typical SR-like curve of the contrast as shown in Fig. 3 can be observed while still enough atoms are left in the trap. To answer this question, we integrate the equations of motion (8) starting from a pure BEC with $\mathbf{s}(0)/n(0)=(\sqrt{3}/2,0,1/2)$ and $n(0)=100$ particles. Figure 4(a) shows the relaxation of the contrast for $J=4\ \mathrm{s}^{-1}$ and $T_1=1$ s. The steady-state value is nearly reached after $t=1$ s when still 40% of the atoms are left in the trap. Figure 4(b) shows the development of the contrast $\alpha(J)$ in time. It is observed that the characteristic SR-like maximum is already well developed after 1 s, where roughly half of the atoms are lost. Thus we conclude that the SR-like maximum of the contrast should be observable in ongoing experiments.

The stochastic resonance effect introduced above is robust and generally not altered by changes in the system parameters or in the presence of weak interparticle interactions. For instance, a change in the bias ϵ of the on-site energies of the two wells preserves the general shape of $\alpha(1/T_1,J)$ shown in Fig. 3 and especially the existence of a pronounced SR-like maximum. At most, the function $\alpha(1/T_1,J)$ is stretched, shifting the position of the SR-like maximum. This shift is illustrated in Fig. 5(a) where we have plotted the contrast as a function of J for the dissipation rate $T_1^{-1}=2\ \mathrm{s}^{-1}$ and different values of ϵ. Thus, this effect provides a useful tool to shift the maximum to values of J, which are easier accessible in ongoing experiments.

Similarly, the position of the maximum of the coherence $\alpha(J)$ is shifted in the presence of weak interparticle interactions. An interacting BEC will usually not show a simple exponential decay of form (14) because the instantaneous decay rate depends on the effective interaction strength $Un(t)$, which also decreases [44–46]. However, the discussion of quasi-steady-states and instantaneous decay rates is still useful if the decay is weak. In this case the system can follow the quasi-steady-states adiabatically and the decay of the population is given by

$$\frac{dn(t)}{dt} = -\kappa(n(t))n(t)$$

and

$$\frac{d\mathbf{s}(t)}{dt} = -\kappa(n(t))\mathbf{s}(t), \tag{20}$$

in good approximation. Substituting this ansatz into the equations of motion (8) yields four coupled nonlinear algebraic equations, which can be disentangled with a little algebra. For a given number of particles n, the instantaneous decay rate κ is obtained by solving the fourth-order algebraic equation,

$$[(\kappa-T_2^{-1})^2+(Un)^2(\kappa-T_1^{-1})^2][(\kappa-T_1^{-1})^2-f_a^2T_1^{-2}] + 4J^2f_a^2T_1^{-2}(\kappa-T_1^{-1})(\kappa-T_2^{-1})=0. \tag{21}$$

The Bloch vector for the corresponding quasi-steady-state is then given by

$$s_{x0}=\frac{\kappa-T_1^{-1}}{\kappa-T_2^{-1}}\frac{(\kappa-T_1^{-1})^2-f_a^2T_1^{-2}}{2Jf_a^2T_1^{-2}}Un^2,$$

$$s_{y0}=\frac{(\kappa-T_1^{-1})^2-f_a^2T_1^{-2}}{2Jf_aT_1^{-1}}n,$$

$$s_{z0}=\frac{\kappa-T_1^{-1}}{f_aT_1^{-1}}n. \tag{22}$$

The fourth-order equation [Eq. (21)] yields four solutions for the decay rate κ. Discarding unphysical values, one finds either one or three quasi-steady-states. This appearance of novel nonlinear stationary states has been discussed in detail

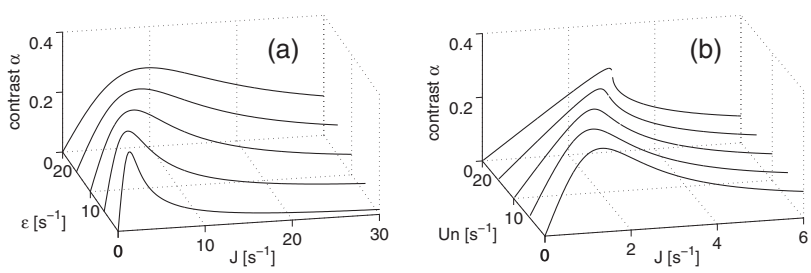

FIG. 5. Steady state values of the contrast α as a function of the tunneling rate (a) for $U=0$ and different values of the energy bias ϵ and (b) as a function of the effective interaction strength $g=Un$ for $\epsilon=0$. The remaining parameters are $\gamma_p=5\ \mathrm{s}^{-1}$ and $T_1^{-1}=2\ \mathrm{s}^{-1}$.

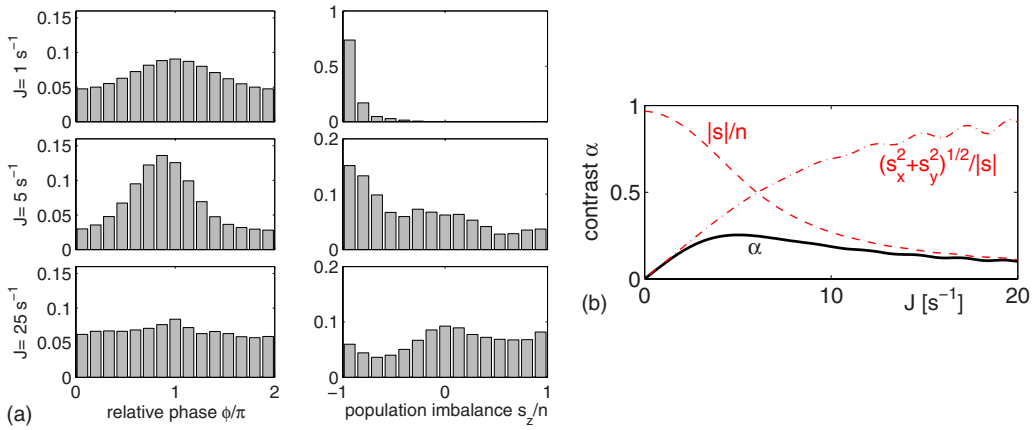

FIG. 6. (Color online) (a) Histogram of the probabilities to measure the relative phase ϕ and the relative population imbalance s_z in a single experimental run after $t=1.5$ s obtained from a MCWF simulation of the many-body dynamics. The initial state was chosen as a pure BEC (i.e., a product state) with $s_z=n/2$ and $n(0)=100$ particles and the remaining parameters are $\gamma_p=5$ s^{-1}, $T_1=0.5$ s, $\epsilon=10$ s^{-1}, and $U=0.1$ s^{-1}. (b) Average contrast $\alpha=\sqrt{s_x^2+s_y^2}/n$ (solid black line) after $t=1.5$ s compared to $\sqrt{s_x^2+s_y^2}/|\mathbf{s}|$ and $|\mathbf{s}|/n$ (dashed red lines).

in the context of nonlinear Landau-Zener tunneling [44–50] and nonlinear transport [51,52].

The resulting contrast $\alpha(J)$ in a quasi-steady-state is shown in Fig. 5(b) for different values of the effective interaction constant $g=Un$. One observes that the position of the SR-like maximum of the contrast is shifted to larger values of the tunneling rate, while the height remains unchanged. Furthermore the shape of the stochastic resonance curve $\alpha(J)$ is altered, becoming flatter for $J<J_{\max}$ and steeper for $J>J_{\max}$. For even larger values of the interaction constant Un one finds a bifurcation into three distinct quasi-steady-states as introduced above. This case will be discussed in detail in Sec. V.

The reasons for the occurrence of an SR-like maximum of the contrast in terms of the underlying many-particle dynamics are illustrated in Fig. 6. To obtain these results we have simulated the dynamics generated by the master equation [Eq. (7)] using the Monte Carlo wave-function (MCWF) method [53–55] averaging over 100 quantum trajectories. For a given particle number n, the probabilities P to obtain the population imbalance s_z and the relative phase ϕ in a projective measurement are thereby given by

$$P(s_z)=\mathrm{tr}(|s_z\rangle\langle s_z|\hat{\rho})$$

and

$$P(\phi)=\mathrm{tr}(|\phi\rangle\langle\phi|\hat{\rho}), \tag{23}$$

where the $\hat{L}_z$ eigenstates

$$|s_z\rangle=|n/2-s_z,n/2+s_z\rangle$$

with

$$s_z=-n/2,-n/2+1,\ldots,n/2 \tag{24}$$

and the phase eigenstates

$$|\phi\rangle:=\frac{1}{\sqrt{n+1}}\sum_{s_z=-n/2}^{+n/2}e^{i\phi s_z}|s_z\rangle$$

with

$$\phi=0,2\pi\frac{1}{n+1},\ldots,2\pi\frac{n}{n+1} \tag{25}$$

each form a complete basis.

Part (a) of Fig. 6 shows a histogram of the probabilities to observe the relative population imbalance s_z/n and the relative phase ϕ in a single experimental run for three different values of the tunneling rate J after the system has relaxed to the quasi-steady-state. With increasing J, the atoms are distributed more equally between the two wells so that the single shot contrast increases. Within the mean-field description this is reflected by an increase in $\sqrt{s_x^2+s_y^2}/|\mathbf{s}|$ at the expense of $|s_z|/|\mathbf{s}|$ [cf. part (b) of the figure]. However, this effect also makes the system more vulnerable to phase noise so that the relative phase of the two modes becomes more and more random and $|\mathbf{s}|/n$ decreases. The average contrast (11) then assumes a maximum for intermediate values of J as shown in part (b) of the figure.

IV. STOCHASTIC RESONANCE OF A DRIVEN BEC

So far we have demonstrated a stochastic resonance of the contrast for a BEC in a static double-well trap with biased particle losses. In the following we will show that the system's response to a weak external driving also assumes a maximum for a finite dissipation rate—an effect which is conceptually closer to the common interpretation of stochastic resonance. From a mathematical viewpoint, however, one can rather relate the *undriven* case discussed above to the stochastic resonance effect in nuclear-magnetic resonance [41]. In fact, the Bloch equations for the magnetization have constant coefficients in the rotating wave approximation and should thus be compared to the undriven equations of motion (8).

Let us consider the response of the system to a weak sinusoidal driving of the tunneling rate

$$J(t)=J_0+J_1\cos(\omega t) \tag{26}$$

at the resonance frequency $\omega=\sqrt{J_0^2+\epsilon^2}$, while the amplitude of the driving is small and fixed as $J_1/J_0=10\%$. A variation

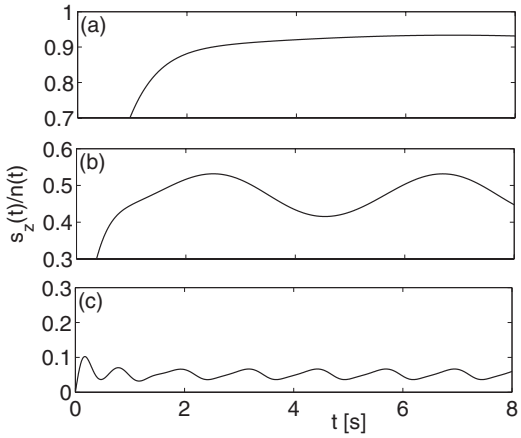

FIG. 7. Dynamics of the relative population imbalance $s_z(t)/n(t)$ in a weakly driven double-well trap for three different values of the tunneling rate: (a) $J_0=0.5\ \mathrm{s}^{-1}$, (b) $J_0=1.5\ \mathrm{s}^{-1}$, and (c) $J_0=5\ \mathrm{s}^{-1}$. The amplitude of the forced oscillations is maximal for intermediate values of J_0 as shown in part (b). The remaining parameters are $T_1^{-1}=2\ \mathrm{s}^{-1}$, $U=0$, $\epsilon=0$, $\gamma_p=5\ \mathrm{s}^{-1}$, and $J_1/J_0=10\%$. Please note the different scalings.

in J can be realized in a quite simple way in an optical setup [21–23], where the tunneling barrier between the two wells is given by an optical lattice formed by two counterpropagating laser beams. A variation in the intensity of the laser beams then directly results in a variation in the tunneling rate J. Figure 7 shows the resulting dynamics for $T_1=0.5$ s and three different values of J_0 and $U=0$. After a short transient period, the relative population imbalance $s_z(t)/n(t)$ oscillates approximately sinusoidally. One clearly observes that the response, i.e., the amplitude of the forced oscillations, assumes a maximum for intermediate values of J_0 matching the external time scale of the dissipation given by T_1^{-1}.

For a detailed quantitative analysis of this stochastic resonance effect, we evaluate the amplitude of the oscillation based on a linear-response argument for $U=0$. In the following, we will use a complex notation for notational convenience, while only the real part is physically significant. The equations of motion (8) are then rewritten in matrix form as

$$\frac{d}{dt}\begin{pmatrix}\mathbf{s}\\ n\end{pmatrix}=(\mathbf{M}_0+\mathbf{M}_1e^{i\omega t})\begin{pmatrix}\mathbf{s}\\ n\end{pmatrix}. \tag{27}$$

The matrices M_0 and M_1 are defined by

$$\mathbf{M}_0=\begin{pmatrix} T_2^{-1} & 2\epsilon_0 & 0 & 0\\ -2\epsilon_0 & T_2^{-1} & -2J_0 & 0\\ 0 & 2J_0 & T_1^{-1} & f_aT_1^{-1}\\ 0 & 0 & f_aT_1^{-1} & T_1^{-1}\end{pmatrix} \tag{28}$$

and

$$\mathbf{M}_1=\begin{pmatrix} 0 & 0 & 0 & 0\\ 0 & 0 & -2J_1 & 0\\ 0 & 2J_1 & 0 & 0\\ 0 & 0 & 0 & 0\end{pmatrix}. \tag{29}$$

As before we consider the dynamics after all transient oscillations have died out, assuming that $\mathbf{s}(t)$ as well as $n(t)$ decay

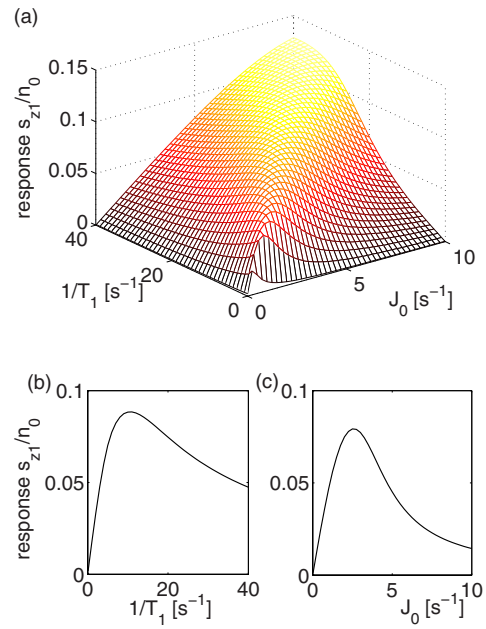

FIG. 8. (Color online) (a) Response [amplitude of the oscillations of $s_z(t)/n(t)$] of a weakly driven double-well trap vs T_1^{-1} and J_0 calculated within linear-response theory. (b) For a fixed value of the tunneling rate $J_0=2.5\ \mathrm{s}^{-1}$. (c) For a fixed value of the dissipation rate $T_1^{-1}=2\ \mathrm{s}^{-1}$. The remaining parameters are $U=0$, $\epsilon=0$, $\gamma_p=5\ \mathrm{s}^{-1}$, and $J_1/J_0=10\%$.

exponentially at the same rate. However, we now also have an oscillating contribution so that we make the ansatz,

$$\mathbf{s}(t)=(\mathbf{s}_0+\mathbf{s}_1e^{i\omega t})e^{-\kappa t},$$

$$n(t)=(n_0+n_1e^{i\omega t})e^{-\kappa t}. \tag{30}$$

The amplitude of the oscillations, i.e., the system response, is thus directly given by $\mathbf{s}_1/n_0$. Substituting this ansatz in the equations of motion and dividing by $e^{-\kappa t}$ yields

$$-\kappa\begin{pmatrix}\mathbf{s}_0\\ n_0\end{pmatrix}+(i\omega-\kappa)\begin{pmatrix}\mathbf{s}_1\\ n_1\end{pmatrix}e^{i\omega t}$$
$$=[\mathbf{M}_0+\mathbf{M}_1e^{i\omega t}]\left[\begin{pmatrix}\mathbf{s}_0\\ n_0\end{pmatrix}+\begin{pmatrix}\mathbf{s}_0\\ n_0\end{pmatrix}e^{i\omega t}\right]. \tag{31}$$

Neglecting the higher order terms $\sim e^{2i\omega t}$ in a linear-response approximation and dividing Eq. (33) in the time-dependent and the time-independent parts yields the equations

$$[-\mathbf{M}_0+(i\omega-\kappa)\mathbb{1}]\begin{pmatrix}\mathbf{s}_1\\ n_1\end{pmatrix}=\mathbf{M}_1\begin{pmatrix}\mathbf{s}_0\\ n_0\end{pmatrix} \tag{32}$$

and Eq. (15), which determine $\mathbf{s}_1$ and n_1. The resulting values of the system response are shown in Fig. 8. One observes the characteristic signatures of a stochastic resonance: if one of the two parameters J_0 and T_1 is fixed, the response assumes a maximum for a finite value of the remaining parameter as shown in parts (b) and (c) of the figure. Part (a) shows that this maximum is assumed if the external (T_1^{-1}) and the internal (J_0) timescales are matched similar to the undriven

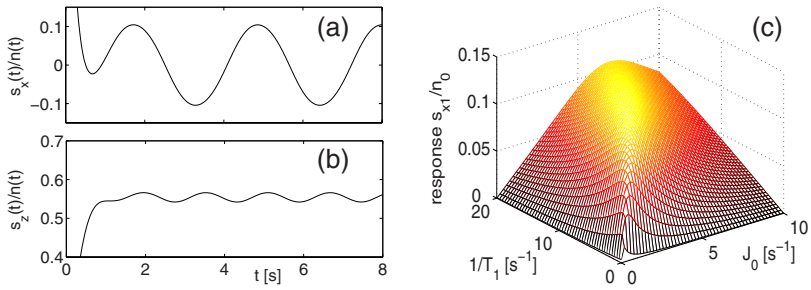

FIG. 9. (Color online) Dynamics of the coherence (a) $s_x(t)/n(t)$ and the relative population imbalance (b) $s_z(t)/n(t)$ for a double-well trap with a driven energy bias ϵ for $J_0=2$ s^{-1} and $T_1^{-1}=4$ s^{-1}. (c) Response [amplitude of the oscillations of $s_x(t)/n(t)$] vs T_1^{-1} and J_0 calculated within linear-response theory. The remaining parameters are $U=0$, $\epsilon_1=1$ s^{-1}, and $\gamma_p=5$ s^{-1}.

case illustrated in Fig. 3. Let us stress that this scenario is again not fundamentally altered in the case of weak interactions as numerically tested but not shown here.

A different situation arises if the energy bias is driven instead of the tunneling rate J such that

$$\epsilon(t) = \epsilon_1 \cos(\omega t). \tag{33}$$

As above we can evaluate the amplitude of the forced oscillations within the linear-response theory, however, with

$$\mathbf{M}_1 = \begin{pmatrix} 0 & -2\epsilon_1 & 0 & 0 \\ 2\epsilon_1 & 0 & 0 & 0 \\ 0 & 0 & 0 & 0 \\ 0 & 0 & 0 & 0 \end{pmatrix}. \tag{34}$$

Solving Eqs. (32) and (15) then yields $s_{1y}=s_{1z}=0$. Remarkably, a driving of the energy bias does not affect the population imbalance in leading order. Only the first component of the Bloch vector s_x, and thus also the contrast α, is strongly affected.

This is illustrated in Figs. 9(a) and 9(b) where the relative population imbalance $s_z(t)/n(t)$ and the first component of the Bloch vector $s_x(t)/n(t)$ are plotted for $J_0=2$ s^{-1}, $T_1^{-1}=4$ s^{-1}, and $\epsilon_1=1$ s^{-1}. The coherence oscillates strongly at the fundamental frequency ω, while the population imbalance oscillates only with a tiny amplitude at the second-harmonic frequency 2ω. The oscillation amplitude of the coherence then again shows the familiar SR-like dependence on the parameters J_0 and T_1 as illustrated in Fig. 9(c).

V. DISSIPATION-INDUCED COHERENCE IN A STRONGLY INTERACTING BEC

Let us finally discuss the case of strong interactions, which is experimentally most relevant and theoretically most profound. This is the regime of the current experiments [21–23], which confirm the theoretical predictions using the two-mode approximation (1) extremely well. However, the model assumes that the ground-state properties of the individual potentials are only slightly affected by the interactions, such that the condition $UN \ll \hbar\omega_{\text{trap}}$ discussed above must be fulfilled. Moreover, the results presented here are not directly applicable to the case of extended trapping potentials, where longitudinal excitations cause dephasing and a loss of purity.

An example for the dynamics of a strongly interacting BEC is shown in Fig. 10(a) for an initially pure BEC with $s_z=n/2$, calculated both with the MCWF method and within the mean-field approximation (8). One observes that the purity p and the contrast α first drop rapidly due to the phase noise and, more importantly, due to the interactions. This is an effect well known from the nondissipative system and can be attributed to a dynamical instability which also leads to the breakdown of the mean-field approximation [32,33,35,56]. However, a surprising effect is found at intermediate times: the purity p is restored almost completely and the contrast α is slightly increasing.

Most interestingly, the observed values of the purity and the coherence are much larger than in the cases where one of the two effects—interactions and dissipation—is missing. The time evolutions for these two cases are also shown in Fig. 10. In the case of no interactions both purity and coherence rapidly drop to values of almost zero and do not revive. This case has been discussed in detail in Sec. III. In the interacting case without dissipation one observes regular revivals, which are artifacts of the small particle number in the simulation and become less pronounced with increasing par-

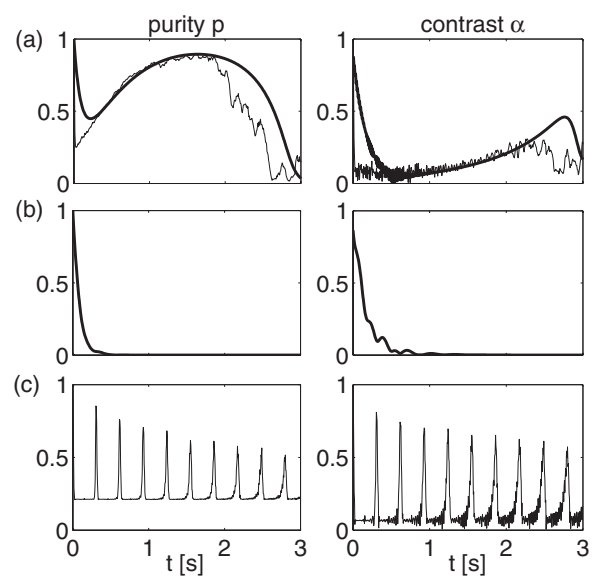

FIG. 10. (a) Time evolution of the purity p and the contrast α for $J=U=10$ s^{-1}, $\epsilon=0$, and $T_1=0.5$ s. (b) Time evolution without interactions ($U=0$) and (c) without dissipation ($1/T_1=1/T_2=0$) for comparison. The occasional revivals are artifacts of the small particle number. The initial state is a pure BEC with $s_z=n/2$ and $n(0)=100$ particles. The results of a MCWF simulation averaged over 100 runs are plotted as a thin solid line in (a) and (c), while the mean-field results are plotted as a thick line in (a) and (b). Note that the mean-field approximation is exact in case (b), whereas it breaks down in case (c) and is thus not shown (cf. [32,35]).

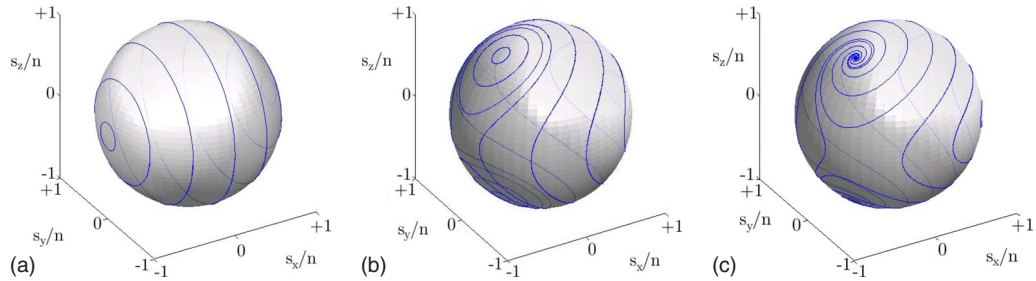

FIG. 11. (Color online) Mean-field dynamics (a) without interactions and dissipation, (b) with interactions $Un=40\ \mathrm{s}^{-1}$, and (c) with interactions and dissipation $\gamma_a=10\ \mathrm{s}^{-1}$. The remaining parameters are $J=10\ \mathrm{s}^{-1}$ and $\epsilon=0$. To increase the visibility we have plotted the rescaled Bloch vector $\mathbf{s}/n$ and we have artificially fixed the particle number so that $n=\mathrm{const}$.

ticle number. Apart from these occasional revivals, however, the purity and the coherence relax to values which are much smaller than in the interacting and dissipative case.

The surprising repurification of a strongly interacting BEC by particle dissipation can be understood within a semiclassical phase-space picture. In order to visualize the effects of particle loss, we have plotted the "classical" phase-space structure generated by the Bloch equation [Eq. (8)] for $\gamma_p=0$ in Fig. 11 without interactions and dissipation (a), with interactions (b), and with both (c). For illustrative purposes, we have plotted the rescaled Bloch vector $\mathbf{s}/n$ and have artificially fixed the particle number so that $n=\mathrm{const}$. Since we are interested only in the short-time dynamics of the Bloch vector and not in the decay of the particle number on longer time scales, this is an appropriate treatment. Moreover, in the quantum jump picture this approximation corresponds to the periods of constant particle number between two loss processes [40,53,55].

Parts (a) and (b) of the figure show the phase-space structure without dissipation and $Un=0$ and $Un=4J$, respectively. One observes the familiar self-trapping bifurcation of the fixed points for $Un>2J$ [31,32]. The phase-space structure is significantly altered in the presence of particle loss as shown in part (c). The most important consequence is the occurrence of an attractive and a repulsive fixed point instead of the elliptic fixed points in the dissipation-free case [40].

In the course of time the system will thus relax to the attractive stationary state illustrated Fig. 11(c). A many-particle quantum state can now be represented by a quasidistribution function on this classical phase space, for instance, the Husimi Q function [34,35]. In this picture, a pure BEC is represented by a maximally localized distribution function and the loss of purity corresponds to a broadening or distortion of the Q function. The existence of an attractive fixed point clearly leads to the contraction of a phase-space distribution function and thus to a repurification of the many-particle quantum state as observed in Fig. 10(a).

However, this nonlinear stationary state exists only as long as the particle number exceeds a critical value given by (cf. [40])

$$U^2n^2 \gtrsim 4J^2 - f_a^2 T_1^{-2}. \tag{35}$$

As particles are slowly lost from the trap, the particle number eventually falls below the critical value. For this reason the attractive fixed point vanishes and the purity drops to the values expected for the linear case $U=0$. Since the attractive fixed point tends toward the equator maximizing $s_x/|\mathbf{s}|$, the contrast assumes a maximum just before the disappearance of the attractive fixed point, while the purity is still large. In Fig. 10(a) this happens after approximately 2.5 s.

The surprising effect of the repurification of a BEC is extremely robust—it is present as long as condition (35) is satisfied. A variation in the system parameters does not destroy or significantly weaken the effect, it only changes the time scales of this relaxation process. Figure 12 compares the time evolution of the purity and the contrast for three different values of the particle loss rate T_1^{-1}. With increasing losses, the nonlinear stationary state is reached much faster but is also lost earlier. One can thus maximize the purity or the contrast at a given point of time by engineering the loss rate. This effect is further illustrated in Fig. 13, where the purity and the contrast after 2 s of propagation are shown in dependence of the loss rate T_1^{-1}. Both curves assume a maximum for a certain finite value of T_1^{-1}.

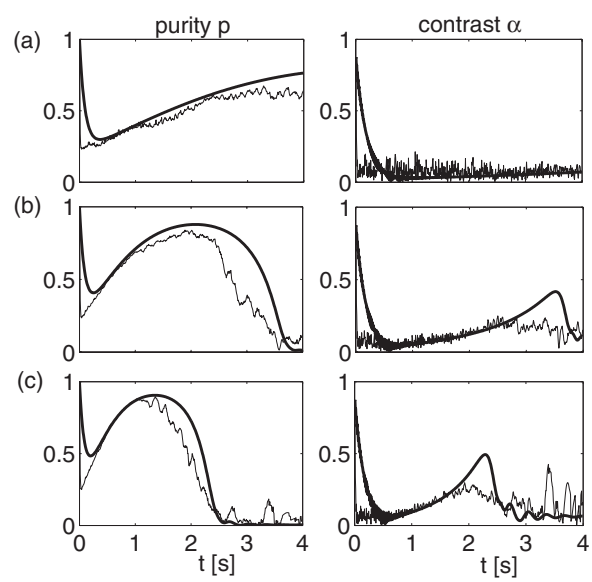

FIG. 12. Time evolution of the purity p and the contrast α for $J=U=10\ \mathrm{s}^{-1}$, $\epsilon=0$, and (a) $1/T_1=0.5\ \mathrm{s}^{-1}$, (b) $1/T_1=1.5\ \mathrm{s}^{-1}$, and (c) $1/T_1=2.5\ \mathrm{s}^{-1}$. The initial state is a pure BEC with $s_z=n/2$ and $n(0)=100$ particles. The results of a MCWF simulation averaged over 100 runs are plotted as a thin solid line, while the mean-field results are plotted as a thick line.

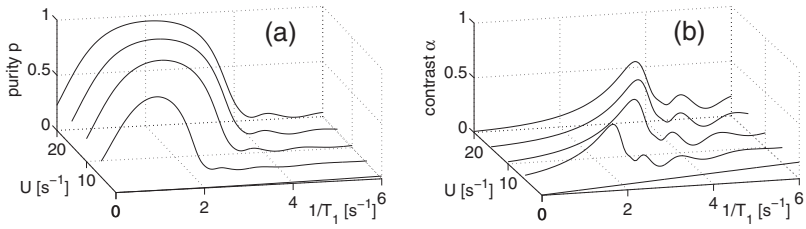

FIG. 13. (a) Purity p and (b) contrast α after $t=2$ s as a function of the dissipation rate $1/T_1$ for different values of the interaction strength Un calculated within the mean-field approximation. The remaining parameters are chosen as in Fig. 10(a).

VI. CONCLUSION AND OUTLOOK

In summary, we have shown that the coherence properties of a weakly and, in particular, also of a strongly interacting Bose-Einstein condensate in a double-well trap can be controlled by engineering the system's parameters and dissipation simultaneously. Surprisingly, dissipation can be used to stimulate coherence in the system rather than—as may be expected—solely reduce it.

In the weakly interacting case, the contrast of the quasi-steady-state of the system assumes a maximum for a finite value of the tunneling and the dissipation rate. This stochastic resonance effect is robust against parameter variations. A Monte Carlo wave-function simulation of the full many-body quantum dynamics shows a good agreement to the mean-field description and provides a microscopic explanation of the observed effect. Moreover, a similar effect can be observed in the case where either the tunneling or the energy bias is driven, which is conceptually even closer to the common interpretation of stochastic resonance.

In Sec. V, we have studied the effects of dissipation on the strongly interacting system. An important conclusion is that the interplay of interactions and dissipation can drive the system to a state of maximum coherence, while both processes alone usually lead to a loss of coherence. We show that this effect can be understood from the appearance of an attractive fixed point in the mean-field dynamics reflecting the metastable behavior of the many-particle system.

Since the double-well BEC is nowadays routinely realized with nearly perfect control on atom-atom interactions and external potentials [21–23], we hope for an experimental verification of the predicted stochastic resonance effect. An interesting perspective is to lift our results to extended dissipative setups as, e.g., studied in [28,29]. Besides the general idea of controlling many-body dynamics [57], one may also investigate the possibility of dynamically engineering entanglement in similar systems as to some extend possible in state-of-the-art experiments [58].

ACKNOWLEDGMENTS

We thank M. K. Oberthaler, J. R. Anglin, and A. S. Sørensen for stimulating discussions. This work has been supported by the German Research Foundation (DFG) (Grant No. WI 3415/1) and the Heidelberg Graduate School of Fundamental Physics (Grant No. GSC 129/1), as well as the Studienstiftung des deutschen Volkes.

[1] R. Benzi, A. Sutera, and A. Vulpiani, J. Phys. A **14**, L453 (1981).
[2] K. Wiesenfeld and F. Moss, Nature (London) **373**, 33 (1995).
[3] M. I. Dykman, D. G. Luchinsky, R. Mannella, P. V. E. McClintock, N. D. Stein, and N. G. Stocks, Nuovo Cimento D **17**, 661 (1995).
[4] L. Gammaitoni, P. Hänggi, P. Jung, and F. Marchesoni, Rev. Mod. Phys. **70**, 223 (1998).
[5] T. Wellens, V. Shatokhin, and A. Buchleitner, Rep. Prog. Phys. **67**, 45 (2004).
[6] R. Löfstedt and S. N. Coppersmith, Phys. Rev. Lett. **72**, 1947 (1994).
[7] R. Löfstedt and S. N. Coppersmith, Phys. Rev. E **49**, 4821 (1994).
[8] A. Buchleitner and R. N. Mantegna, Phys. Rev. Lett. **80**, 3932 (1998).
[9] T. Wellens and A. Buchleitner, J. Phys. A **32**, 2895 (1999).
[10] S. F. Huelga and M. B. Plenio, Phys. Rev. A **62**, 052111 (2000).
[11] H. H. Adamyan, S. B. Manvelyan, and G. Y. Kryuchkyan, Phys. Rev. A **63**, 022102 (2001).
[12] S. F. Huelga and M. B. Plenio, Phys. Rev. Lett. **98**, 170601 (2007).
[13] Y. Khodorkovsky, G. Kurizki, and A. Vardi, Phys. Rev. Lett. **100**, 220403 (2008).
[14] Yun Li, Y. Castin, and A. Sinatra, Phys. Rev. Lett. **100**, 210401 (2008).
[15] B. Kraus, H. P. Büchler, S. Diehl, A. Kantian, A. Micheli, and P. Zoller, Phys. Rev. A **78**, 042307 (2008).
[16] S. Diehl, A. Micheli, A. Kantian, B. Kraus, H. P. Büchler, and P. Zoller, Nat. Phys. **4**, 878 (2008).
[17] F. Verstraete, M. M. Wolf, and J. I. Cirac, e-print arXiv:0803.1447.
[18] N. Syassen, D. M. Bauer, M. Lettner, T. Volz, D. Dietze, J. J. Garcia-Ripoll, J. I. Cirac, G. Rempe, and S. Dürr, Science **320**, 1329 (2008).
[19] J. J. Garcia-Ripoll, S. Dürr, N. Syassen, D. M. Bauer, M. Lettner, G. Rempe, and J. I. Cirac, New J. Phys. **11**, 013053 (2009).
[20] D. Witthaut, F. Trimborn, and S. Wimberger, Phys. Rev. Lett. **101**, 200402 (2008).
[21] M. Albiez, R. Gati, J. Fölling, S. Hunsmann, M. Cristiani, and M. K. Oberthaler, Phys. Rev. Lett. **95**, 010402 (2005).
[22] R. Gati, B. Hemmerling, J. Fölling, M. Albiez, and M. K. Oberthaler, Phys. Rev. Lett. **96**, 130404 (2006).

[23] R. Gati, J. Estève, B. Hemmerling, T. B. Ottenstein, J. Appmeier, A. Weller, and M. K. Oberthaler, New J. Phys. **8**, 189 (2006).
[24] S. Fölling, S. Trotzky, P. Cheinet, M. Feld, R. Saers, A. Widera, T. Müller, and I. Bloch, Nature (London) **448**, 1029 (2007).
[25] S. Trotzky, P. Cheinet, S. Fölling, M. Feld, U. Schnorrberger, A. M. Rey, A. Polkovnikov, E. A. Demler, M. D. Lukin, and I. Bloch, Science **319**, 295 (2008).
[26] T. Schumm, S. Hofferberth, L. M. Andersson, S. Wildermuth, S. Groth, I. Bar-Joseph, J. Schmiedmayer, and P. Krüger, Nat. Phys. **1**, 57 (2005).
[27] J. R. Anglin, Phys. Rev. Lett. **79**, 6 (1997).
[28] S. Hofferberth, I. Lesanovsky, B. Fischer, T. Schumm, and J. Schmiedmayer, Nature (London) **449**, 324 (2007).
[29] S. Hofferberth, I. Lesanovsky, T. Schumm, J. Schmiedmayer, A. Imambekov, V. Gritsev, and E. Demler, Nat. Phys. **4**, 489 (2008).
[30] G. J. Milburn, J. Corney, E. M. Wright, and D. F. Walls, Phys. Rev. A **55**, 4318 (1997).
[31] A. Smerzi, S. Fantoni, S. Giovanazzi, and S. R. Shenoy, Phys. Rev. Lett. **79**, 4950 (1997).
[32] A. Vardi and J. R. Anglin, Phys. Rev. Lett. **86**, 568 (2001).
[33] J. R. Anglin and A. Vardi, Phys. Rev. A **64**, 013605 (2001).
[34] F. Trimborn, D. Witthaut, and H. J. Korsch, Phys. Rev. A **77**, 043631 (2008).
[35] F. Trimborn, D. Witthaut, and H. J. Korsch, Phys. Rev. A **79**, 013608 (2009).
[36] J. Ruostekoski and D. F. Walls, Phys. Rev. A **58**, R50 (1998).
[37] D. F. Walls and G. J. Milburn, Phys. Rev. A **31**, 2403 (1985).
[38] C. W. Gardiner and P. Zoller, *Quantum Noise*, Springer Series in Synergetics (Springer, Berlin, 2004).
[39] I. Bloch, T. W. Hänsch, and T. Esslinger, Phys. Rev. Lett. **82**, 3008 (1999).
[40] F. Trimborn, D. Witthaut, and S. Wimberger, J. Phys. B **41**, 171001 (2008).
[41] L. Viola, E. M. Fortunato, S. Lloyd, C.-H. Tseng, and D. G. Cory, Phys. Rev. Lett. **84**, 5466 (2000).
[42] F. Bloch, Phys. Rev. **70**, 460 (1946).
[43] A. J. Leggett, Rev. Mod. Phys. **73**, 307 (2001).
[44] S. Wimberger, R. Mannella, O. Morsch, E. Arimondo, A. R. Kolovsky, and A. Buchleitner, Phys. Rev. A **72**, 063610 (2005).
[45] P. Schlagheck and T. Paul, Phys. Rev. A **73**, 023619 (2006).
[46] P. Schlagheck and S. Wimberger, Appl. Phys. B: Lasers Opt. **86**, 385 (2007).
[47] Biao Wu and Qian Niu, Phys. Rev. A **61**, 023402 (2000).
[48] Biao Wu and Jie Liu, Phys. Rev. Lett. **96**, 020405 (2006).
[49] D. Witthaut, E. M. Graefe, and H. J. Korsch, Phys. Rev. A **73**, 063609 (2006).
[50] E. M. Graefe, H. J. Korsch, and D. Witthaut, Phys. Rev. A **73**, 013617 (2006); E. M. Graefe, H. J. Korsch, and A. E. Niederle, Phys. Rev. Lett. **101**, 150408 (2008).
[51] T. Paul, K. Richter, and P. Schlagheck, Phys. Rev. Lett. **94**, 020404 (2005).
[52] K. Rapedius, D. Witthaut, and H. J. Korsch, Phys. Rev. A **73**, 033608 (2006).
[53] J. Dalibard, Y. Castin, and K. Mølmer, Phys. Rev. Lett. **68**, 580 (1992).
[54] K. Mølmer, Y. Castin, and J. Dalibard, J. Opt. Soc. Am. B **10**, 524 (1993).
[55] H. J. Carmichael, *An Open Systems Approach to Quantum Optics* (Springer, Berlin, 1993).
[56] M. Cristiani, O. Morsch, N. Malossi, M. Jona-Lasinio, M. Anderlini, E. Courtade, and E. Arimondo, Opt. Express **12**, 4 (2004).
[57] J. Madroñero, A. Ponomarev, A. R. R. Carvalho, S. Wimberger, C. Viviescas, A. Kolovsky, K. Hornberger, P. Schlagheck, A. Krug, and A. Buchleitner, Adv. At. Mol. Opt. Phys. **53**, 33 (2006).
[58] J. Estève, C. Gross, A. Weller, S. Giovanazzi, and M. K. Oberthaler, Nature (London) **455**, 1216 (2008).